Photogeneration and recombination processes of neutral and charged excitations in films of a ladder-type poly(*para*-phenylene)

M. Wohlgenannt
Department of Physics, University of Utah, Salt Lake City, Utah 84112
and Institut für Festkörperphysik, Technische Universität Graz, Petersgasse 16, A-8010 Graz, Austria

W. Graupner
Department of Physics, Virginia Tech, Blacksburg, Virginia 24061-0435
and Institut für Festkörperphysik, Technische Universität Graz, Petersgasse 16, A-8010 Graz, Austria

G. Leising
Institut für Festkörperphysik, Technische Universität Graz, Petersgasse 16, A-8010 Graz, Austria

Z. V. Vardeny
Department of Physics, University of Utah, Salt Lake City, Utah 84112
(Received 25 February 1999)

We introduce a version of the cw photomodulation technique, measured far from the steady state, for obtaining the quantum efficiency, η, of long-lived photoexcitations in π-conjugated polymers. We apply this technique to films of a ladder-type poly(*para*-phenylene) [mLPPP] for studying the photogeneration action spectra, $\eta(E)$, and recombination kinetics of photogenerated neutral and charged excitations such as singlet and triplet excitons and charged polarons. Whereas the $\eta(E)$ spectrum for singlet excitons shows a step function increase at a photon energy, E, close to the optical gap ($\simeq 2.6$ eV), both triplet and polaron $\eta(E)$ spectra show, in addition, a monotonous rise at higher E. The rise for triplets is explained by singlet exciton fission into triplet pairs, and from a model fit we get the triplet exciton energy ($\simeq 1.6$ eV). For polarons this rise is modeled by an electron intersegment tunneling process. The electroabsorption spectrum is also measured and analyzed in terms of Stark shift of the lowest lying exciton, $1B_u$, and enhanced oscillator strength of the important mA_g exciton. A consistent picture for the lowest excited state energy levels and optical transitions in the neutral (singlet and triplet) and charged manifolds is presented. From both the exciton binding energy of $\simeq 0.6$ eV and the singlet-triplet energy splitting of $\simeq 1$ eV, we conclude that the e-e interaction in mLPPP is relatively strong. Our results are in good agreement with recent *ab initio* band structure calculations for several π-conjugated polymers. [S0163-1829(99)13531-8]

I. INTRODUCTION

The photogeneration dynamics of singlet excitons and secondary photoexcitations, such as triplets and polarons, in π-conjugated polymers have usually been measured by picosecond (ps) transient spectroscopic techniques rather than cw spectroscopies, since their photogeneration processes usually occur in the subnanosecond time domain.[1] On the other hand, the excited states energy levels are often measured in these polymers by cw optical techniques, including electroabsorption[2,3] and resonant Raman scattering,[4–6] and by two and three photon nonlinear optical spectroscopies.[7,8] In this paper we introduce a version of cw photomodulation action spectroscopy, which is capable of measuring the photogeneration dynamics of secondary photoexcitations without the need of ps transient optical techniques. This technique uses the excitation dependence (action spectrum) of various photoinduced absorption (PA) bands in the photomodulation spectrum, measured under conditions far from the steady state.

We have used the PA action spectrum technique to obtain the photogeneration quantum efficiency, η, and its dependencies on temperature, θ, and excitation photon energy, E, for singlet and triplet excitons and polarons, respectively, in films of methyl substituted ladder-type poly(*para*-phenylene) [mLPPP] (Fig. 1, inset). mLPPP is an attractive π-conjugated polymer for blue-light emitting diodes[9,10] (see Fig. 1) and photopumped lasers[11,12] due to its high photoluminescence quantum yield; this is caused in part, by the intrachain order in the film induced by the planarization of neighboring phenyl rings[13] (Fig. 1 inset). We found that whereas the action spectrum for the photoluminescence quantum efficiency comprises a step-function response at E close to the optical gap, $E_{op} \simeq 2.6$ eV, the $\eta(E)$ spectrum for both triplet exciton and polaron PA bands also contains a monotonous rise at $E > E_{op}$. For triplet excitons this rise is interpreted as due to singlet exciton fission into triplet pairs, and from a model fit to the experimental data we get the triplet energy, $E_T \simeq 1.6$ eV. The rise in the $\eta(E)$ spectrum of polarons at high energies is explained by a hot exciton dissociation process via electron intersegment tunneling. We also measured the electroabsorption spectrum and analyze it in terms of electric field induced changes of odd and even parity excitons. From these measurements a consistent picture of the most important excited energy levels and optical transitions is constructed.

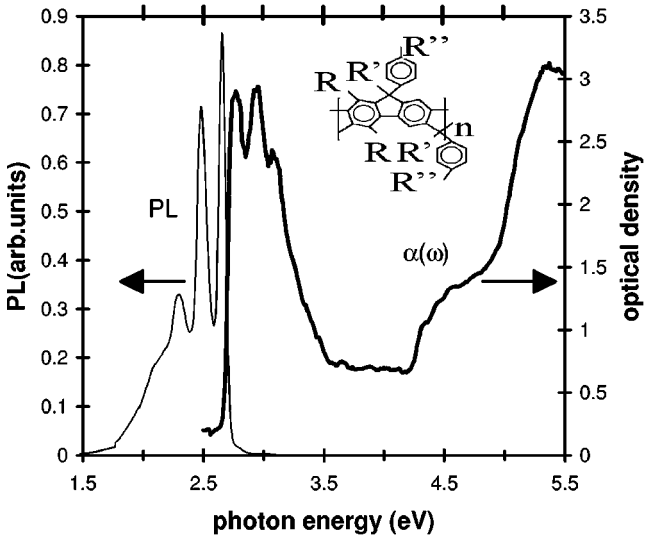

FIG. 1. Photoluminescence (PL, solid) and absorption [$\alpha(\omega)$, bold] spectra of mLPPP. Inset shows the mLPPP repeat unit.

II. EXPERIMENT

Our method is based on the cw photomodulation (PM) technique. For the excitation beam we used either an Ar^+ laser at several discrete photon energies, E, or a monochromatized Xenon lamp to continuously vary E, between 2 and 4.5 eV. The excitation beam was modulated with a chopper at frequencies, f, between 10 and 4 kHz. A combination of various incandescent lamps (tungsten halogen and glowbar), diffraction gratings, optical filters, and solid state detectors (silicon, germanium, indium antimonide, and mercury cadmium teluride) was used to span the probe photon energy, $\hbar\omega$, between 0.1 and 3 eV. The PM spectrum vs $\hbar\omega$ was obtained by dividing the pump beam induced changes in the probe beam transmission, $\Delta T(\omega)$, by the probe beam transmission, $T(\omega)$, where ΔT was measured by a phase sensitive technique; in this case the PA, or $\Delta\alpha$ ($=-d^{-1}\Delta T/T$, where d is the film thickness) does not depend on the system energy response. ΔT was measured in our studies as a function of pump excitation intensity, I, modulation frequency, f, and temperature, θ. To obtain the quantum efficiency per absorbed photon we multiplied I by the factor $g(E)=1/(Ed)(1-R)[1-\exp(-\alpha d)]$, where $R(E)$ and $\alpha(E)$ are the film reflectivity and absorption coefficient, respectively.

The PA, or $\Delta\alpha$, is proportional to the photoexcitation density, N, via the relation $\Delta\alpha=N\sigma$, where σ is the excitation optical cross section. Since $\Delta\alpha\sim\Delta T$, it follows that the changes in the probe transmission measured in phase, ΔT_{in}, and quadrature, ΔT_Q, to the laser beam modulation may be directly related to N dynamics, where $\Delta T_{\text{in}}\sim N_{\text{in}}$ and $\Delta T_Q\sim N_Q$. The two N components, N_{in} and N_Q, may be obtained, in principle, from the modulated excitation intensity $I(t)$, which is a periodic square wave in time with an illuminating pulse duration $t_0=1/2f$, where f is the laser modulation frequency, using either the monomolecular (MR) or bimolecular (BR) rate equation:

$$\frac{dN}{dt}=\eta g I-\beta N \quad \text{(MR)}, \tag{1}$$

TABLE I. Photoexcitation density N in the photomodulation measurements for monomolecular (MR) and bimolecular recombination (BR) kinetics in the limits of steady state and far from the steady state. N_{in}, N_Q are the in-phase and quadrature photoexcitation densities, respectively. gI gives the density of absorbed photons, η is the photogeneration quantum efficiency, τ is the MR photoexcitation decay time, and γ is the bimolecular recombination constant.

Recombination kinetics	Steady state	Far from the steady state
Monomolecular	$N_{\text{in}}=\eta g I\tau/2$	$N_{\text{in}}=O[1/(\tau f^2)]$
	$N_Q=O(\tau^2 f)$	$N_Q=\eta g I/4\pi f$
Bimolecular	$N_{\text{in}}=\sqrt{\eta g I/2\gamma}$	$N_{\text{in}}=O[1/(\tau f^2)]$
	$N_Q=O(\tau^2 f)$	$N_Q=\eta g I/4\pi f$

$$\frac{dN}{dt}=\eta g I-\gamma N^2 \quad \text{(BR)}. \tag{2}$$

In Eqs. (1) and (2), β and γ are the MR and BR constants, which are related to the photoexcitation decay time τ by $\tau=1/\beta$ and $\tau=1/(\gamma N)$, respectively. We calculated (see the appendix and Table I) complete analytic expressions for the two N components for the MR kinetics, and analytic expressions for the BR kinetics in the limiting cases of steady state ($f\tau\ll 1$) and far from the steady state ($f\tau\gg 1$). Moreover, the exact numerical results for the BR kinetics were also obtained. As a particularly important result of these calculations we found that far from the steady state, namely $f\tau\gg 1$,

$$N_Q=\frac{Ig\eta}{4\pi f}, \tag{3}$$

independent of τ and the recombination kinetics. The decay time τ depends on the type of recombination kinetics and on various external parameters such as temperature and most importantly in the case of BR kinetics, on the excitation density. Since the excitation density strongly varies in the experiment (it is determined by the lamp intensity, the grating efficiency, the sample reflectivity and absorption coefficient dependencies on E) then the absence of τ in the above expression for N_Q is essential for the direct determination of η from cw measurements. Thus, when measuring N_Q far from the steady state, studies of the photoexcitation generation process via the E and θ dependencies of η can be readily achieved with cw techniques. We note that in previous studies,[14–16] $N_{\text{in}}(f)$ and $N_Q(f)$ were analyzed for both MR and BR kinetics; however, that N_Q for $f\tau\gg 1$ does not depend on τ was not realized and thus basically ignored. Therefore, it has been generally believed that cw techniques cannot be used to directly study η for various photoexcitations since, in contrast to N_Q (see the appendix), N_{in} depends on τ, which, in turn, depends on E and θ. This is, however, not the case if N_Q is measured far from the steady state [Eq. (3)].

We summarize the results of our calculations for N_{in} and N_Q in Table I. Also, the characteristic properties of $N_{\text{in}}(f)$ and $N_Q(f)$ are demonstrated in Fig. 2, where the calculated $N_Q(f)$ and $N_{\text{in}}(f)$ normalized by $G=g\eta I$, are plotted for both MR and BR, respectively, with two different recombi-

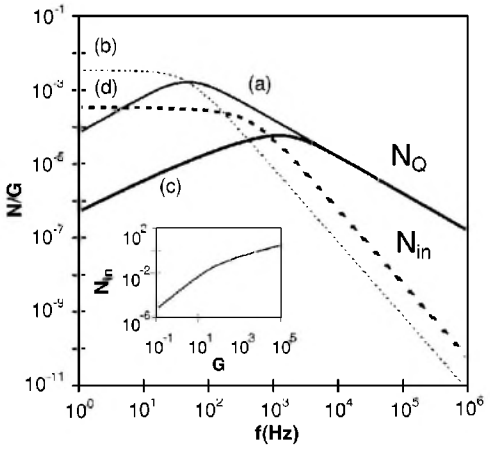

FIG. 2. The two photoexcitation density components N_Q and N_{in} normalized by the absorbed photon density G, calculated vs modulation frequency f. Curves (a) and (b) are for MR, and curves (c) and (d) are for BR; solid (dotted) lines are for N_Q (N_{in}). The recombination constants are $\beta = 300$ Hz and $\gamma N = 1$ kHz, for the MR and BR kinetics, respectively. The inset shows N_{in} vs G calculated for BR kinetics with $\gamma N = 1$ kHz and $f = 100$ Hz.

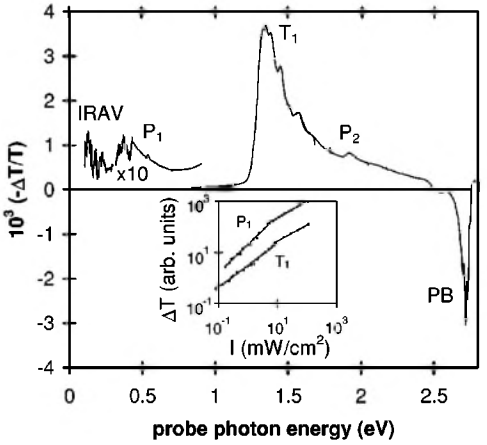

FIG. 3. The in-phase photomodulation spectrum of a mLPPP film at 80 K, excited at 3.5 eV and modulated at 100 Hz. The triplet (T_1), polaron (P_1 and P_2), IR active vibrations (IRAV) and photobleaching (PB) bands are assigned. The inset shows the dependencies of T_1 and P_1 PA bands on the excitation intensity I, where the lines are power laws with exponents close to 1 and 0.5, respectively.

nation rates. Firstly, it is seen in Fig. 2 that $N_{\text{in}} = N_Q$ at f_0, such that $f_0\tau \simeq 1$, for both recombination processes. Secondly, at $f \gg f_0$, $N_Q \sim 1/f$, whereas $N_{\text{in}} \sim 1/f^2$, and therefore N_Q dominates $|\Delta T|$ at high f Importantly, $N_Q(f)$ approaches the asymptotic behavior, $1/f$, at large f, *independent of the recombination process and* τ. Thirdly, at $f > f_0$, $N_{\text{in}}(f)$ scales with $1/\tau$, explaining the reason why $N_{\text{in}}(\text{BR}) > N_{\text{in}}(\text{MR})$ at high f, whereas the opposite is true at low f.

To identify the recombination kinetics of various excitations in the PM spectrum, we also calculated $N_{\text{in}}(G)$ at a fixed f (Fig. 2, inset). We found that N_{in} increases linearly with G for the MR kinetics. However, for the BR kinetics we calculated $N_{\text{in}} \sim G^{3/2}$ at low G (where $f\tau \gg 1$) changing at high G (where $f\tau \ll 1$) to $\sqrt{G}$ dependence. We therefore note that the N_{in} vs G plot may serve to identify the photoexcitation recombination kinetics using cw studies, whereas N_Q measured far from the steady state may be used to directly obtain η for the various photoexcitations in the PM spectrum.

The spin state of these excitations may be obtained by the PA detected magnetic resonance (PADMR) technique.[17,18] In PADMR we measure the changes in PA induced by a modulated μ-wave field (in our experiment, 3 GHz) in resonance with the Zeeman split spin-1/2 sublevels in magnetic field H.[17,18] The μ-wave resonant absorption leads to small changes, δT, in T. This δT is proportional to δN induced by the μ waves, caused by changes in spin-dependent recombination rates. Two types of PADMR spectra are possible:[18] The H-PADMR spectrum, in which δT is measured at a fixed probe wavelength λ as the magnetic field H is scanned, and the λ-PADMR spectrum, in which δT is measured at a constant H, in resonance, while λ is scanned.

The measurements in this paper were done on a mLPPP film that was drop-cast from a toluene solution on a sapphire substrate and its optical density, (OD), at the laser wavelength was ≈ 1 (Fig. 1).

III. RESULTS AND DISCUSSION

In Fig. 1 we show the polymer repeat unit, the optical absorption, $\alpha(\omega)$ and photoluminescence (PL) spectra of the mLPPP film used here. At low photon energies, $\alpha(\omega)$ consists of a three peak structure at 2.75, 2.93, and 3.11 eV, respectively, that we interpret as an optical transition into the lowest odd parity exciton ($1B_u$) and its two phonon replica $\simeq 180$ meV apart. The PL spectrum is much sharper than $\alpha(\omega)$, but otherwise also contains a pronounced three peak feature, which is Stokes shifted from that in $\alpha(\omega)$ by about 0.1 eV. Using an integrating sphere, we measured the absolute PL quantum efficiency in mLPPP to be about 30%. At high photon energies, $\alpha(\omega)$ also contains absorption bands at 4.5 and 5.3 eV, respectively, that are interpreted as due to transitions into higher, but more localized excitons.[19]

A. PM spectrum

In Fig. 3 we show the PM spectrum of a drop-cast mLPPP film at $\theta = 80$ K excited at $E = 3.5$ eV. The PM spectrum is dominated by the PA band T_1 at 1.3 eV and also by the two correlated PA bands: P_1 and P_2 at 0.4 and 1.9 eV, respectively. A series of photoinduced infrared active vibrations (IRAV's) that are correlated by their f and θ dependencies with the PA bands P_1 and P_2, but not with T_1, are also seen at $\hbar\omega < 0.25$ eV.[20,21] The photobleaching (PB) feature in Fig. 3 marks the mLPPP optical gap, $E_{\text{op}} \simeq 2.6$ eV,[22] which can also be deduced from the PL band onset at high $\hbar\omega$ (Fig. 1). The photoinduced IRAV's indicate that charge carriers are photogenerated in the polymer chains. Their correlation with P_1 and P_2, but not with T_1 shows, therefore, that the former bands are due to long-lived *charged* excitations, whereas the latter band is caused by long-lived *neutral* excitations.

B. PADMR spectroscopy

The H-PADMR spectrum of mLPPP at $\hbar\omega = 1.9$ eV is shown in Fig. 4(a), inset. We observe a negative resonance at

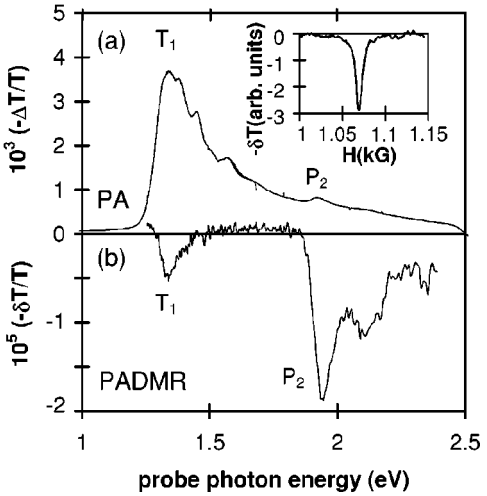

FIG. 4. PA spectrum (a) compared to λ-PADMR spectrum (b) of spin-1/2 excitations, measured at $H=1065$ G ($g=2$) and 10 K. The inset shows the H-PADMR spectrum at 1.9 eV.

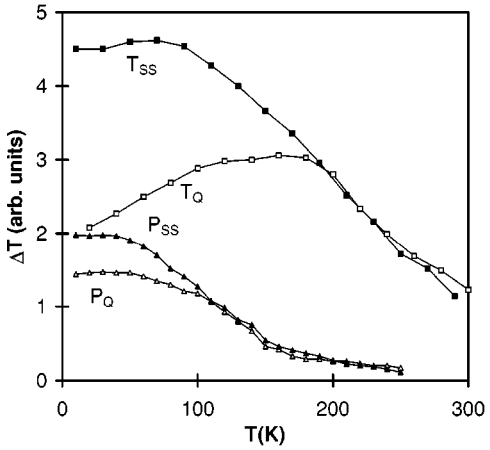

FIG. 5. Temperature dependencies of T_1 and P_1 PA bands, both at steady state conditions (measured in-phase, 15 Hz chopping frequency and 1 W/cm^2 pump intensity), denoted T_{SS} and P_{SS}, respectively, and far from steady state conditions (measured at quadrature, 4 kHz, 0.5 W/cm^2 pump intensity), denoted T_Q and P_Q, respectively.

1065 G due to enhanced recombination of spin-1/2 photoexcitations. The λ-PADMR spectrum measured at $H=1065$ G is shown in Fig. 4(b). It contains a sharp band at 1.9 eV, which coincides in energy with the P_2 band [Fig. 4(a)], followed by a phonon replica at 2.1 eV. We note the remarkable ability of PADMR to elucidate small PA bands such as P_2, which are covered by much stronger bands, such as T_1 in the PM spectrum [compare Figs. 4(a) and 4(b)]. The λ-PADMR spectrum also shows that T_1 is much less correlated with spin-1/2 excitations and therefore does not originate from long-lived polarons. We also note that P_1 and P_2 bands, in fact coincide in energy with the two doping induced absorption bands in mLPPP caused by polarons,[20] and that T_1 is close in energy to the long-lived excitations in isolated PPP oligomers assigned to triplets.[21] Based on these facts and the spectroscopies described above, we conclude that P_1 and P_2 PA bands are due to photogenerated *polarons*, whereas T_1 is caused by photoexcited *triplet excitons*. In the following we use these assignments to study the long-lived photoexcitation generation and recombination processes in mLPPP.

The fact that T_1 also shows a negative spin-1/2 resonance, although weak, is interesting by itself and shows that there exists a correlation between polarons and triplet photoexcitations in mLPPP. This may be explained by a model of triplet photogeneration, in which two spin-parallel polarons undergo fusion to become a triplet exciton.[23] This explains why both resonances, at P_2 and T_1, respectively, have the same sign: reducing the density of polarons by magnetic resonance absorption that enhances their recombination rate also results in a reduced density of triplets. However, below we will show that polaron fusion is only a minor channel of triplet photogeneration in mLPPP. One could also try to argue that the spin 1/2 PADMR resonance of the triplet PA band is due to the photobleaching of the ground state, which happens because part of the ground state's oscillator strength is stored in the polaron photoexcitations. However, in this scenario, resonance enhanced recombination of the polarons would reduce photobleaching and thus an increase in triplet density is expected: The T_1 would then show a positive resonance, contrary to that observed in the experiment [Fig. 4(b)].

C. Recombination kinetics

The inset in Fig. 3 shows the dependence of the in-phase PA for the T_1 and P_1 PA bands on the pump laser intensity, measured at 100 Hz. Both bands show a change from a linear dependence at low I to a nearly $\sqrt{I}$. Actually, at high I we measured $\Delta T \sim I^m$, where the exponent $m=0.63$ and 0.67 for triplets and polarons, respectively. We calculated that such a change in the exponent m only occurs for the BR kinetics case [Eq. (2)] (see the appendix). We therefore conclude BR kinetics for both polaron and triplet photoexcitations. BR kinetics is obvious for polaron recombination, $P^+ + P^- \rightarrow ground\ state$. However, it is not trivial for the photogenerated triplet excitons; our results show, therefore, that triplet-triplet annihilation, where $dT_1/dt \sim \gamma T_1^2$ is dominant in mLPPP, in contrast to triplet exciton kinetics in other polymers.[18] We note that the neat, planarized mLPPP backbone structure[13] may increase triplet diffusion in these films, thus promoting BR kinetics. The T_1 and P_1 intensity dependencies allow us to rule out polaron fusion as a major channel of triplet photogeneration. Polaron fusion, described above, is a bimolecular generation process (not to be confused with BR), from which it follows that the triplet density depends quadratically on the polaron density; consequently there should be a quadratic relation between their respective PA bands, which is not observed in the experiment.

Figure 5 shows the temperature dependencies of the PA, $\Delta T(\theta)$ of triplets and polarons for both the steady state (SS), T_{SS}, and P_{SS}, respectively, where the PA is measured in-phase at 15 Hz and $I=100$ mW, and also far from the steady state, T_Q and P_Q, respectively, where the PA is measured in quadrature at 4 kHz and $I=50$ mW. For triplet ΔT it is seen that for $\theta<200$ K the temperature dependencies of T_{SS} and T_Q are different from each other. However, the two ΔT have similar θ dependencies at $\theta>200$ K, where steady

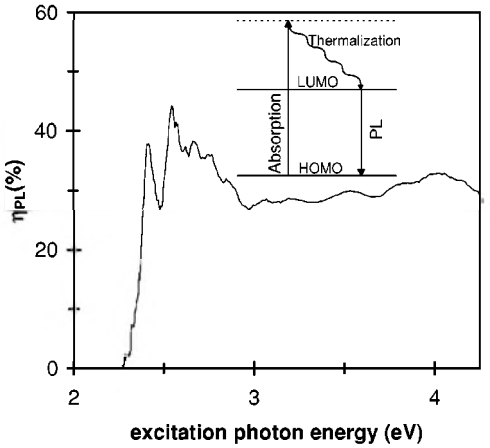

FIG. 6. PL quantum efficiency, η_{PL} vs excitation photon energy. The inset shows that the cw PL is obtained following hot exciton thermalization.

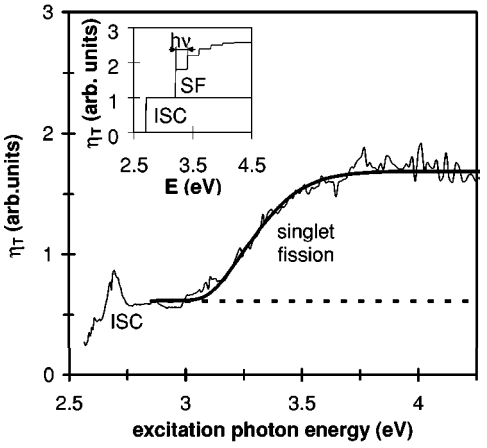

FIG. 7. Photogeneration quantum efficiency spectrum, $\eta_T(E)$, of the triplet excitons in mLPPP. The bold line through the data points is a theoretical fit using a model of singlet fission (SF). ISC is the process of triplet photogeneration via intersystem crossing. The dotted line illustrates the separation of $\eta_T(E)$ into the two processes. The inset shows an idealized $\eta_T(E)$ spectrum with no inhomogeneous broadening (see text), where $h\nu$ is a vibrational quantum.

state conditions ($f\tau \leq 1$) are attained. The reason is that at $\theta > 200$ K, $\Delta T_{in}(\theta)$ and $\Delta T_Q(\theta)$ are both governed by the temperature dependence of the decay time $\tau(\theta)$ (Table I). Moreover, we note that T_Q increases with θ for $\theta < 200$ K. Since far from the steady state, T_Q is proportional to the photogeneration quantum efficiency η [Eq. (3)], then the increase of T_Q is caused by an increase of η with θ; an unusual η property that we can uniquely pick up using our PM technique. For the polarons, both $P_Q(\theta)$ and $P_{SS}(\theta)$ fall on top of each other already for $\theta > 100$ K , demonstrating that the polaron density is mostly determined by $\tau(\theta)$, whereas the temperature dependence of the generation process itself is much weaker. Indeed, it has been shown[24] that the temperature dependence of the PA due to charge excitations in mLPPP can be modeled using only the directly, experimentally determined activation energies of traps in mLPPP. Taken together, these results show that the photogeneration quantum efficiency of polarons is temperature independent, in agreement with subnanosecond transient photoconductivity measurement in many other π-conjugated polymers.[25–28]

D. Action spectroscopy

We used the photogeneration action spectrum technique to measure $\eta(E)$ for the PL band and T_1 and P_1 PA bands in mLPPP.

1. PL action spectrum

By measuring the PL/(Ig) dependence on the excitation energy, E, we obtained the PL quantum efficiency, $\eta_{PL}(E)$ as shown in Fig. 6. We normalized $\eta_{PL}(E)$ by the absolute value of η_{PL} measured using an integrating sphere, and found $\eta_{PL} \approx 30\%$ at $E = 3.5$ eV. It is seen in Fig. 6 that $\eta_{PL}(E)$ abruptly increases at $E \approx 2.4$ eV, followed by a constant value at higher E. This step-function behavior is similar to that measured in the best poly(phenylene-vinylene) (PPV) films,[29] and shows that singlet excitons are the primary excitations in mLPPP, as can be also inferred from the large exciton binding energy (≈ 0.5 eV) obtained for this polymer.[22] PL mostly occurs following the thermalization of the original hot exciton down to the lowest lying singlet exciton (Fig. 6, inset): Hot excitons thermalize on a timescale of the order of a ps, whereas the PL emission from thermalized excitons typically occurs on the order of 100 ps following the excitation.[30] Thus, the singlet exciton recombines radiatively with a given quantum efficiency independent of the original excitation energy. Consequently, the PL action spectrum reflects the photogeneration quantum efficiency spectrum for singlet excitons, which is close to 1 in mLPPP, independent of E.

2. Triplet action spectrum

At longer times, however, triplet excitons are formed in mLPPP, as may be concluded from the existence of the T_1 PA band in Fig. 3. By measuring the $\Delta T_Q/(\mathrm{Ig})$ dependence on E for the T_1 band at low I (where $f\tau \gg 1$), we obtained the triplet quantum efficiency, $\eta_T(E)$ as shown in Fig. 7. Again, $\eta_T(E)$ has a step function response at $E \approx E_{op}$ similar to $\eta_{PL}(E)$; however, $\eta_T(E)$ increases at higher E, reaching a plateau at $E \approx 3.7$ eV. It is thus apparent that triplet generation occurs via two main processes. The first process is associated with the generation of thermalized singlet excitons and therefore has a similar E dependence as that of $\eta_{PL}(E)$ in Fig. 6. We identify this process as due to intersystem crossing, ISC, from the singlet to the triplet manifold, which occurs following exciton thermalization at times of order 1 ns,[30,31] and hence its flat response with E for $E \geq E_{op}$. The other process, with an onset at $E \simeq 3.2$ eV, is therefore due to hot excitons and must thus occur at least on the timescale of the hot exciton thermalization. Both upper excited state transfer[32] (UEST) and singlet exciton fisson[33] (SF) mechanisms for triplet generation have onsets above the optical gap. UEST has its maximum efficiency at E close to higher energy triplet states. Then the beginning of the plateau in Fig. 7 should mark the energy of the second lowest triplet exciton state. This energy (≈ 3.7 eV), however, is higher than that of the mAg singlet exciton, which was measured to be at $\simeq 3.3$ eV,[22] (see also Sec. III E) and thus UEST cannot explain our data. We therefore identify the second triplet

photogeneration process as SF ($Ex \rightarrow T\uparrow + T\downarrow$), which is operative at $E \geqslant 2E_T$, where E_T is the triplet energy. We thus obtain from the higher $\eta_T(E)$ onset at 3.2 eV a value $E_T \simeq 1.6$ eV.

The theoretical prediction for the singlet fission quantum efficiency spectrum is a step function response with the step at $2E_T$.[33] But the $\eta_T(E)$ spectrum does not show such a sharp step function response (Fig. 7). On the contrary, the rise prior to reaching the plateau is spread out in energy over several tenths of eV. We therefore introduce a model (see also Ref. 34) that is able to explain the shape of this broad rise in energy and get the E_T value in spite of this broad spectrum. Our model follows two main ideas: (i) Singlet fission, just like any other electronic transition, may be accompanied by emission of strongly coupled vibrations. (ii) E_T is not a single energy, but is spread out due to inhomogeneous broadening, which we denote as $E_T(x)$, where the variable x describes an inhomogeneous parameter, such as conjugation length, for example.

Thus, the energy E necessary to produce a triplet exciton is given by

$$E = E_T(x) + ph\nu_P, \tag{4}$$

where p is the number of emitted phonons and ν_P is the vibrational frequency. The relative strength of the emission of p phonons during the electronic transition is described by the Huang-Rhys formula:[35]

$$h(p) = \frac{S^p}{p!}. \tag{5}$$

Figure 7 inset illustrates the model: For a weak inhomogeneity the SF action spectrum would comprise several steps. The nth step marks the onset of the photogeneration of a triplet pair accompanied by the emission of n vibrational quanta.

To quantify the inhomogenous broadening we have fitted the optical absorption band of mLPPP with an asymmetric Gaussian distribution.[2] Let us call the distribution resulting from this fit $D'(E)$, where $D(E)$ is the distribution obtained by summing up over the vibronic progressions. $D(E)$ is then given by[2]

$$D(E) = \sum_{p=0}^{\infty} h(p) D'(E + ph\nu_P). \tag{6}$$

Singlet fission produces pairs of triplet excitons on neighboring chains or neighboring chain segments. Then the energy E to produce a triplet pair and coupled vibrations is given by

$$E = E_T(x_1) + p_1 h\nu_P + E_T(x_2) + p_2 h\nu_P, \tag{7}$$

where the distributions $E_T(x_1) = E_T(x_2)$, $p_1(p_2)$ is the number of emitted phonons in connection with the generation of the first (second) triplet exciton. Next, we convoluted $D(E)$ for the two triplet excitons to obtain the distribution D_{pair} describing the inhomogenous distribution and phonon emission related to the generation of a triplet pair with energy E_{pair}:

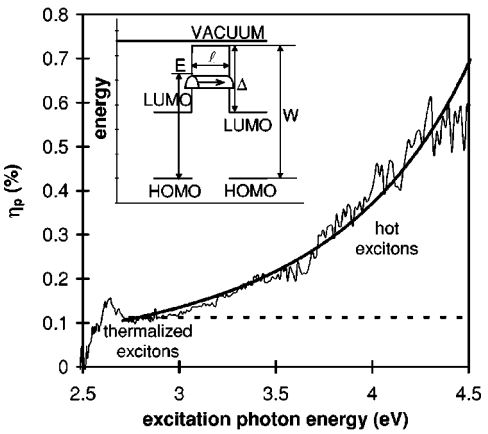

FIG. 8. Photogeneration quantum efficiency spectrum, $\eta_P(E)$, of polaron excitations in mLPPP; the two photogeneration processes due to hot and thermalized excitons, respectively, are assigned. The dotted line illustrates the separation of $\eta_P(E)$ into the two processes. The line through the data points is a theoretical fit using an intersegment tunneling model, as explained in the inset. HOMO (LUMO) is the highest occupied (lowest unoccupied) molecular orbital, l (Δ) is the intersegment barrier potential width (height), and W is the energy difference between the HOMO and the vacuum level.

$$D_{\text{pair}}(E_{\text{pair}}) = \int_{E_1=0}^{E_{\text{pair}}} D(E_1) D(E_{\text{pair}} - E_1) dE_1. \tag{8}$$

We get the triplet photogeneration quantum efficiency, η_T, by convoluting D_{pair} with a step function having an onset at $E = E_{\text{pair}}$.

$$\begin{aligned} \eta_T(E) &= \int_{E_{\text{pair}}=0}^{\infty} D_{\text{pair}}(E_{\text{pair}}) H(E - E_{\text{pair}}) dE_{\text{pair}}, \\ &= \int_{E_{\text{pair}}=0}^{E} D_{\text{pair}}(E_{\text{pair}}) dE_{\text{pair}}, \\ &= \int_{E_{\text{pair}}=0}^{E} \int_{E_1=0}^{E_{\text{pair}}} D(E_1) D(E_{\text{pair}} - E_1) dE_1 dE_{\text{pair}}, \end{aligned} \tag{9}$$

which finally results in

$$\eta_T(E) = \int_{E_2=0}^{E} \int_{E_1=0}^{E-E_2} D(E_1) D(E_2) dE_1 dE_2, \tag{10}$$

where $E_2 = E_{\text{pair}} - E_1$.

Equation (10) contains E_T and S as the only two fitting parameters since $D(E)$ is directly extracted from $\alpha(\omega)$. The excellent fit to the experimental $\eta_T(E)$ curve shown in Fig. 7 was obtained using Eq. (10) with $E_T = 1.6$ eV and $S = 0.15$. From this measurement we note that the singlet-triplet energy difference $\Delta_{ST} = E_S - E_T$ is approximately 1 eV for the lowest exciton ($1B_u$), and that similar values for Δ_{ST} were also measured in PPV,[36] as well as calculated by recent *ab initio* band structure calculations.[37]

3. Polaron action spectrum

In Fig. 8 we show the polaron photogeneration quantum efficiency, $\eta_P(E)$ obtained by measuring $\Delta T_Q(E)/(Ig)$ for

the P_1 PA band (Fig. 3), and normalizing it by the doping induced absorption cross section, σ, of polarons.[20] It is seen that $\eta_P(E)$ abruptly increases at $E=2.5$ eV, similar to $\eta_{PL}(E)$ and $\eta_T(E)$ in Figs. 6 and 7, respectively. At $E>2.85$ eV, however, $\eta_P(E)$ monotonously increases with E, where a saturation at high E similar to that found for $\eta_T(E)$ in Fig. 7 is not observed. It is again obvious that $\eta_P(E)$ is composed from two contributions related to two different polaron photogeneration processes. One process is due to thermalized excitons and is thus independent of E, similar to $\eta_{PL}(E)$ (Fig. 6). We identify this process as exciton dissociation ($EX \rightarrow P^- + P^+$) at impurities and defects in the film, which occurs *following* hot exciton thermalization, similar to the "extrinsic" process observed in cw photoconductivity (PC).[38–40] The second polaron photogeneration process showing a distinctive E dependence is related to *hot* excitons and is thus intrinsic in nature.[41] To explain this temperature independent, intrinsic process we suggest an electron tunneling model (Fig. 8 inset), as follows:

The electron and hole of a thermalized exciton are closely bound by a binding energy of ≈ 0.6 eV (see Sec. III E). This makes their separation into free charges (polarons) very unlikely; soon after its thermalization the exciton will recombine to the ground state. We argue that this immediate recombination can only be prevented by separating the electron and hole to neighboring chain segments during the exciton thermalization. We therefore suggest that at initially high E the electron may tunnel to another chain segment, before its excess energy is completely released. The tunneling probability for the electron, $p(E)$, is given by

$$p(E)=\nu_0 \int_{E_{op}}^{E} e^{-2l/\hbar \sqrt{2m_e^*(\Delta+E_{op}-E')}} dE', \qquad (11)$$

where l is the tunneling barrier thickness, m_e^* is the electronic effective mass, and Δ is the barrier height for tunneling; here $\Delta+E_{op}=W$, where W is the polymer highest occupied molecular orbital (HOMO)-vacuum energy difference (see Fig. 8, inset); ν_0 is the number of tunneling attempts per unit energy as the electron thermalizes from E to E_{op}. The integrand in Eq. (11) is the standard WKB formula for the tunneling probability through a square potential barrier. As polaron photogeneration happens during the thermalization process, the tunneling probability is integrated over the thermalization time, where ν_0—assumed to be a constant—establishes the connection between the time and energy scale. This tunneling model is in agreement with the directly determined time evolution (with 100 fs resolution) of the exciton dissociation probability in mLPPP,[42] which is one order of magnitude higher during hot exciton thermalization as compared to thermalized excitons. The following values for ν_0, W, and $l\sqrt{m_e^*}$ are extracted from the fit obtained to both $\eta_P(E)$ *spectrum* and *magnitude* shown in Fig. 8: We obtained $\nu_0=0.5(\text{eV})^{-1}$, $W=5.5\pm0.5$ eV, which is in excellent agreement with electron affinity measurements in mLPPP,[10] $l\sqrt{m_e^*}=4\pm1$ Å $\sqrt{m_e}$. The limits for the intrachain m_e^* value are $0.1m_e$ (conventional inorganic semiconductors) and m_e; for these values of m_e^* we obtained from $l\sqrt{m_e^*}$ determined above $l=12$ and $l=4$ Å, respectively. These values are in agreement with the expected barrier thickness separating two conjugation segments. It is known that the maximum energy relaxation rate $R=\Delta E/\Delta t$ of hot excitons is $R=h\nu^2$,[43] where ν is the most strongly coupled phonon. For mLPPP $h\nu=0.18$ eV ($C=C$ stretching mode), determined from the $\alpha(\omega)$ replica in Fig. 1. We can therefore estimate the attempt frequency for tunneling, ν_T, from the relation

$$\nu_T=R\nu_0. \qquad (12)$$

From $\nu_0=0.5$ eV^{-1} determined above and Eq. (12), we get $\nu_T\approx 0.1\nu$, which is reasonably close to the maximum allowed ν_T ($=\nu$).

After thermalization is completed electron tunneling is not possible any more. Indeed, there is an energy onset to electron tunneling, as it must be at least equal to the difference between exciton and polaron pair binding energies. We note that at electric fields, F, of order 10^5 V/cm, a similar model was used to explain $\eta_{PC}(E)$ at high F,[44] where the electron and hole are separated by a barrier arising from their Coulomb interaction and F.

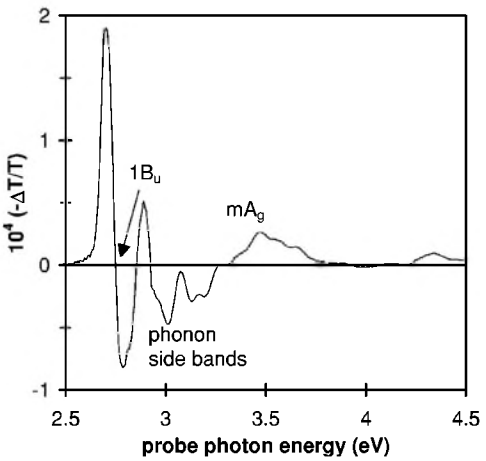

FIG. 9. Electroabsorption spectrum of a mLPPP film at 80 K. The spectral features associated with the Stark shift of the $1B_u$ exciton, its phonon replica, and the mA_g exciton are assigned.

E. Electroabsorption spectrum

To complete the studies of neutral excitations in mLPPP we also measured the electroabsorption (EA) spectrum. The measurements were made using a modulated electric field of up to 1.6×10^5 V/cm. The mLPPP film was deposited on an electrode structured sapphire substrate consisting of interlocking metallic fingers with 20 μm gap. The electric field modulation frequency was 500 Hz, and the changes ΔT in transmission T due to the applied voltage were measured with a lock-in amplifier at $2f$.[2]

The EA spectrum of an mLPPP film at 80 K is shown in Fig. 9 up to 4.5 eV. The spectrum consists of three derivativelike features with peaks at 2.7, 2.88, and 3.06 eV, respectively, and a positive spectral feature with an onset at 3.3 eV;[22] the highest energy bump at 4.3 eV is due to higher excitons in $\alpha(\omega)$ (Fig. 1). Similar spectral features have been observed before in the EA spectra of many π-conjugated polymers[2] and thus we analyze these features according to the standard model using summation over

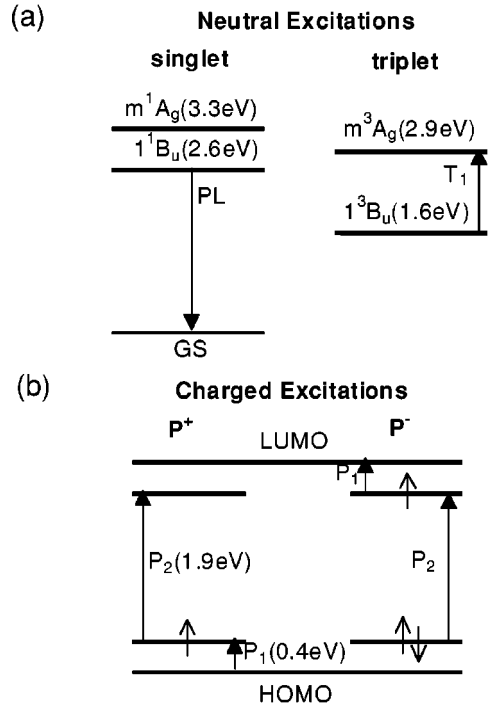

FIG. 10. Schematic representation of the excited states energy levels and optical transitions of the most important excitons with odd (B_u) and even (A_g) parity and polarons in mLPPP. (a) Neutral singlet and triplet manifold. (b) Polaronic levels in the charged manifold for both P^+ and P^-.

states.[2,45] We therefore interpret the derivativelike features in Fig. 9 as due to the Stark shift of the $1B_u$ exciton at $\simeq 2.7$ eV and its two phonon side bands, which are 180 meV apart. The positive spectral feature at higher energy, on the contrary, is interpreted as due to the mA_g exciton at $\simeq 3.3$ eV. We note that the $1B_u$ energy deduced here is averaged over the conjugation length distribution in the film, whereas cw PL is mainly due to the longest chains. This may explain the energy difference between the measured optical gap from the PL onset at 2.6 eV, and the average $1B_u$ exciton at 2.7 eV extracted from the EA spectrum.

F. Excited states energy levels

With these assignments in mind we can now complete the picture of the main excited states energy levels and optical transitions in mLPPP, deduced in this work. This is shown in the schematic representation of Figs. 10(a) and 10(b) for the neutral and charged manifolds, respectively.

In the neutral manifold [Fig. 10(a)] the 1^1B_u at 2.6 eV and the 1^3B_u at 1.6 eV are deduced from the PL band and singlet fission onset, respectively. The m^1A_g level at 3.3 eV is deduced from the onset of the positive feature in the EA spectrum, whereas the m^3A_g level at 2.9 eV is deduced from the T_1 PA band, which theory predicts to be the strongest triplet transition from the 1^3B_u.[45] From these measurements we note that $\Delta_{ST}=E_S-E_T$ is approximately 1 eV for the lowest exciton ($1B_u$) and approximately 0.4 eV for the important mA_g exciton. That Δ_{ST} is smaller for the mA_g exciton is consistent with the more extended wave function of this high energy exciton. It also indicates that the continuum band onset, where presumably the singlet and triplet states are degenerate, is located at a still higher energy. This shows that the exciton binding energy, E_b, defined here as the energy difference between 1^1B_u and the continuum band onset, is at least 0.6 eV in mLPPP, consistent with the relatively strong e-e interaction in this polymer. Also, since Δ_{ST} is determined by the exchange interaction, then the large Δ_{ST} value (≈ 1 eV) for the $1B_u$ exciton obtained from our measurements is in agreement with the strong e-e interaction in mLPPP that we deduced from E_b. We also note that similar values for Δ_{ST} were also measured in PPV,[36] as well as calculated by recent *ab initio* band structure calculations.[37]

The HOMO and lowest unoccupied molecular orbital (LUMO) levels in the charged manifold [Fig. 10(b)] do not have to coincide with those of the neutral manifold. In fact the HOMO-LUMO gap, E_{HL}, in PPV was found[46] to be larger for the charged manifold by about 0.2 eV, compared to the optical gap in the neutral manifold. We may estimate E_{HL} in mLPPP for the charged manifold, if we assume that the polaron levels are symmetrically located in the HL gap, as shown in Fig. 10(b). In this case there exists the following relation:

$$E_{HL}=2P_1+P_2. \tag{13}$$

Using $P_1=0.4$ eV and $P_2=1.9$ eV from the PA bands in Fig. 3, we calculate from Eq. (13) $E_{HL}=2.7$ eV. This is close, but higher than $E_{op}=2.6$ eV found in the singlet manifold. That $E_{op}\approx E_{HL}$ shows that the polaronic relaxation energy associated with charge injection is small in mLPPP and this is consistent with the relatively high quantum yield found for light emitting diodes (LED's) made from mLPPP thin films.

IV. CONCLUSIONS

We studied the photoexcitation dynamics as revealed in PM measurements for the cases of monomolecular and bimolecular recombination kinetics, respectively. In particular, we found that the quadrature PA component solely depends on the photogeneration quantum efficiency, if the measurements are conducted far from the steady state. Thus, studies of subnanosecond generation processes of long-lived photoexcitations can be completed using cw PM rather than transient techniques. We presented the PA and PA detected magnetic resonance spectra of mLPPP thin films. The PA spectrum is dominated by a triplet-triplet absorption at 1.3 eV and by two polaron absorption bands at 0.4 and 1.9 eV, respectively. We showed that the band at 1.9 eV has a strong spin-1/2 resonance, whereas for the PA band at 1.3 eV we found a much weaker spin-1/2 resonance. We proposed a fusion mechanism of two spin-parallel polarons into a triplet to explain the observed triplet spin-1/2 PADMR resonance. The dependencies of the triplet and polaron PA bands on the excitation laser intensity and temperature were measured and analyzed in terms of specific generation and recombination processes. The photogeneration action spectra for the singlet and triplet excitons and polarons were presented. We identified two photogeneration processes for triplets, namely intersystem crossing and singlet fission, and also two photogeneration processes for polarons, namely dissociation at defects and electron intersegment tunneling. From a model fit to the triplet action spectrum we obtained a value for the

triplet exciton energy, $E_T = 1.6$ eV. From fitting the polaron action spectrum we obtained values for the polymer HOMO-vacuum energy difference, $W = 5.5$ eV, and for the width of the tunneling barrier, $4\ \text{Å} < d < 12\ \text{Å}$. From the EA spectrum we found the energy of the two most important excitons in mLPPP, namely $1B_u$ and mA_g. The energy levels and optical transitions of the most important excitons in the singlet and triplet manifolds and polarons in mLPPP were then deduced and their complete scheme was presented. We conclude that e-e interaction in mLPPP is relatively strong.

ACKNOWLEDGMENTS

We thank U. Scherf and K. Muellen for the mLPPP powder, and E. Ehrenfreund, I. Gontia, and R. Österbacka for useful discussions. The work at the University of Utah was supported in part by DOE Grant No. FG-03-96 ER 45490, and NSF Grant No. DMR-9732820. This work was also supported by the Austrian FWF SFB, Elektroaktive Stoffe and P.12806 grants, respectively.

APPENDIX

Assuming that the lock-in amplifier analyzes the first harmonic of $N(t)$, we numerically and analytically solved separately the two rate equations

$$\frac{dN}{dt} = \eta g I - \beta N (MR); \quad \frac{dN}{dt} = \eta g I - \gamma N^2 (BR), \tag{A1}$$

for N_{in} and N_Q at different f and I, spanning the steady state ($f\tau \ll 1$), and far from it ($f\tau \gg 1$). The excitation $I(t)$ is a periodic square wave in time with an illuminating pulse duration $t_0 = 1/2f$, where f is the laser modulation frequency, τ is the photoexcitation decay time, i.e., $\tau = 1/\beta$ and $\tau = 1/(\gamma N)$ for MR and BR kinetics, respectively. An analytic expression for MR kinetics can be obtained by solving the Fourier transform of Eq. (14) for $N(f)$. This gives

$$N(f) = \frac{\eta g I}{2} \frac{\beta}{(2\pi f)^2 + \beta^2} - i \frac{\eta g I}{2} \frac{2\pi f}{(2\pi f)^2 + \beta^2}, \tag{A2}$$

where the real and imaginary parts denote the N_{in} and N_Q components, respectively. We can obtain analytic expressions for BR kinetics in the limiting cases of steady state and far from the steady state. At steady state we set the left-hand side of Eq. (14) to zero and solve for $N(f)$:

$$N_{\text{SS}} = \sqrt{\frac{\eta g I}{2\gamma}}. \tag{A3}$$

Far from steady state (e.g., at high f) the left-hand side of Eq. (14) becomes important because of the time derivative, however, the recombination term will be negligible, as N decreases with f. Under these conditions we can easily solve the Fourier transform of the remaining equation for the component $N_Q(f)$ and get

$$N_Q = -\frac{\eta g I}{4\pi f}. \tag{A4}$$

To get the exact, numerical results for the BR kinetics we first solved Eq. (14) analytically in the time domain and calculated the Fourier component integrals numerically. The various terms and their approximations are given in Table I.

[1] *Primary Photoexcitations in Conjugated Polymers; Molecular Excitons vs. Semiconductor Band Model*, edited by N.S. Sariciftci (World Scientific, Singapore, 1997).
[2] M. Liess, S. Jeglinski, Z.V. Vardeny, M. Ozaki, K. Yoshino, Y. Ding, and T. Barton, Phys. Rev. B **56**, 15 712 (1997).
[3] M. Cardona, *Solid State Physics Supplement 11: Modulation Spectroscopy* (Academic Press, New York, 1969).
[4] M. Ozaki, E. Ehrenfreund, R.E. Benner, T.J. Barton, K. Yoshino, and Z.V. Vardeny, Phys. Rev. Lett. **79**, 1762 (1997).
[5] Z.V. Vardeny, E. Ehrenfreund, O. Brafman, and B. Horovitz, Phys. Rev. Lett. **51**, 2326 (1983).
[6] M. Gussoni, C. Castiglioni, and G. Zerbi, *Spectroscopy of Advanced Materials*, edited by R.J.H. Clark and R.E. Hester (John Wiley & Sons, New York, 1991).
[7] W.S. Fann, S. Benson, J.M.J. Madey, S. Etemad, G.L. Baker, and F. Kajzar, Phys. Rev. Lett. **62**, 1492 (1989).
[8] B. Lawrence, W.E. Torruellas, M. Cha, M.L. Sundheimer, G.I. Stegeman, J. Meth, S. Etemad, and G. Baker, Phys. Rev. Lett. **73**, 597 (1994).
[9] S. Tasch, A. Niko, G. Leising, and U. Scherf, Appl. Phys. Lett. **68**, 1090 (1996).
[10] S. Tasch, E.J.W. List, C. Hochfilzer, G. Leising, P. Schlichting, U. Rohr, Y. Geerts, U. Scherf, and K. Müllen, Phys. Rev. B **56**, 4479 (1997).
[11] C. Zenz, W. Graupner, S. Tasch, G. Leising, K. Müllen, and U. Scherf, Appl. Phys. Lett. **71**, 2566 (1997).
[12] A. Haugeneder, M. Hilmer, C. Kallinger, M. Perner, W. Spirkl, U. Lemmer, J. Feldmann, and U. Scherf, Appl. Phys. B: Lasers Opt. **66**, 389 (1998).
[13] G. Leising, O. Ekstroem, W. Graupner, F. Meghdadi, M. Moser, G. Kranzelbinder, T. Jost, S. Tasch, B. Winkler, L. Athouel, G. Froyer, U. Scherf, K. Muellen, G. Lanzani, M. Nisoli, and S. DeSilvestri, Proc. SPIE **2852**, 189 (1996).
[14] C. Botta, S. Luzzati, R. Tubino, D.D.C. Bradley, and R.H. Friend, Phys. Rev. B **48**, 14 809 (1993).
[15] G. Dellepiane, C. Cuniberti, D. Comoretto, G. Lanzani, G.F. Musso, P. Piaggio, R. Tubino, A. Borghesi, C. Dell'Erba, G. Garbarino, and L. Moramarco, Phys. Rev. B **45**, 6802 (1992).
[16] E. Dekel, E. Ehrenfreund, D. Gershoni, P. Boucaud, I. Sagnes, and Y. Campidelli, Phys. Rev. B **56**, 15 734 (1997).
[17] X. Wei, B.C. Hess, Z.V. Vardeny, and F. Wudl, Phys. Rev. Lett. **68**, 666 (1992).
[18] P. Lane, X. Wei, and Z.V. Vardeny, Phys. Rev. B **56**, 4626 (1997).
[19] M. Chandross, S. Muzumdar, S. Jeglinski, X. Wei, Z.V. Vardeny, E.W. Kwock, and T.M. Miller, Phys. Rev. B **50**, 14 702 (1994).
[20] W. Graupner, M. Mauri, J. Stampfl, G. Leising, U. Scherf, and K. Müllen, Solid State Commun. **91**, 7 (1994).
[21] W. Graupner, S. Eder, M. Mauri, G. Leising, and U. Scherf, Synth. Met. **69**, 419 (1995).

[22] G. Meinhardt, A. Horvath, G. Weiser, and G. Leising, Synth. Met. **84**, 667 (1997).
[23] V. Dyakonov, in *Primary Photoexcitations in Conjugated Polymers; Molecular Excitons vs Semiconductor Band Model* (Ref. 1), p. 254.
[24] W. Graupner, G. Leditzky, and G. Leising, Phys. Rev. B **54**, 7610 (1996).
[25] C.H. Lee, G. Yu, D. Moses, and A.J. Heeger, Phys. Rev. B **49**, 2396 (1994).
[26] D. Moses, M. Sinclair, and A.G. Heeger, Phys. Rev. Lett. **58**, 2710 (1987).
[27] D. Moses, J. Wang, G. Yu, and A.G. Heeger, Phys. Rev. Lett. **80**, 2685 (1998).
[28] D. Moses, H. Okumoto, C.H. Lee, A.J. Heeger, T. Ohnishi, and T. Noguchi, Phys. Rev. B **54**, 4748 (1996).
[29] R.H. Friend, G.J. Denton, J.J.M. Halls, N.T. Harrison, A.B. Holmes, A. Köhler, A. Lux, S.C. Moratti, K. Pichler, N. Tessler, and K. Towns, Synth. Met. **84**, 463 (1997).
[30] S. Frolov, M. Liess, P.A. Lane, W. Gellermann, Z.V. Vardeny, M. Ozaki, and K. Yoshino, Phys. Rev. Lett. **78**, 4285 (1997).
[31] J.W. Blatchford, S.W. Jessen, L.B. Lin, J.J. Lih, T.L. Gustafson, A.J. Epstein, D.K. Fu, M.J. Marsella, T.M. Swager, A.G. MacDiarmid, S. Yamaguchi, and H. Hamaguchi, Phys. Rev. Lett. **76**, 1513 (1996).
[32] M. Pope and C.E. Svenberg, *Electronic Processes in Organic Crystals* (Clarendon Press, Oxford, 1982).
[33] R.H. Austin, G.L. Baker, S. Etemad, and P. Thompson, J. Chem. Phys. **90**, 11 (1989).
[34] M. Wohlgenannt, W. Graupner, R. Österbacka, G. Leising, D. Comoretto, and Z.V. Vardeny, in ICSM 98 Proceedings, edited by P. Bernier, G. Bidan, and S. Lefrant (Elsevier, Amsterdam, in press).
[35] W.V. Houston, Phys. Rev. **57**, 184 (1940).
[36] R. Österbacka, M. Wohlgenannt, D. Chinn, and Z.V. Vardeny, Phys. Rev. B (to be published).
[37] M. Rohlfing and S.G. Louie, Phys. Rev. Lett. **82**, 1959 (1999).
[38] M. Chandross, S. Mazumdar, S. Jeglinski, X. Wei, Z.V. Vardeny, E.W. Kwock, and T.M. Miller, Phys. Rev. B **50**, 14 702 (1994).
[39] S. Barth, H. Bässler, U. Scherf, and K. Müllen, Chem. Phys. Lett. **288**, 147 (1998).
[40] A. Köhler, D.A. Dos Santos, D. Beljonne, Z. Shuai, J-L. Brédas, A.B. Holmes, A. Kraus, K. Müllen, and R.H. Friend, Nature (London) **392**, 903 (1998).
[41] M. Wohlgenannt, W. Graupner, G. Leising, and Z.V. Vardeny, Phys. Rev. Lett. **82**, 3344 (1999).
[42] W. Graupner, G. Cerullo, G. Lanzani, M. Nisoli, E.J.W. List, G. Leising, and S. DeSilvestri, Phys. Rev. Lett. **81**, 3259 (1998).
[43] Z. Vardeny and J. Tauc, in *Semiconductors Probed by Ultrafast Laser Spectroscopy*, edited by R.R. Alfano (Academic Press, New York, 1984), Vol. II, p. 23.
[44] V.I. Arkhipov, E.V. Emelianova, and H. Bässler, Phys. Rev. Lett. **82**, 1321 (1999).
[45] S. Mazumdar and M. Chandross, in *Primary Photoexcitations in Conjugated Polymers; Molecular Excitons vs Semiconductor Band Model* (Ref. 1), p. 384.
[46] I. H. Campbell, T. W. Hagler, D. L. Smith, and J. P. Ferraris, Phys. Rev. Lett. **76**, 1900 (1996).